EMI Filter Design for a 1 MHz, 10 kW Three-Phase/Level PWM Rectifier

Michael Hartmann, *Student Member, IEEE*, Hans Ertl, *Member, IEEE*, and Johann W. Kolar, *Fellow, IEEE*

***Abstract*—The attenuation characteristics of electromagnetic interference (EMI) filters in practice often differ from theoretical predictions and minor changes can result in a significant improvement in performance. The performance of the differential-mode (DM) filter stage can usually be well predicted, but the common mode (CM) behavior is more difficult to handle. This is especially true for three-phase pulsewidth modulation (PWM) rectifier systems, which inherently show a large high-frequency CM voltage at the rectifier output. Possible CM noise current paths of a three-phase/level PWM rectifier are analyzed in this paper where parasitic capacitances to the heat sink and to earth are considered. In addition, a concept to significantly reduce CM emissions is discussed in detail. Based on the proposed models, an EMI filter design for a system with 1 MHz switching frequency is shown. Experimental verification of the designed EMI filter is presented by impedance and conducted emission (CE) measurements taken from a 10 kW prototype. Several practical aspects of filter implementation such as component arrangement, shielding layers, magnetic coupling, etc., are discussed and verified by measurements.**

***Index Terms*—Common mode (CM) noise, electromagnetic compatibility (EMC) filters, power-factor correction (PFC), three-phase ac–dc power conversion.**

I. Introduction

In NEW application fields, e.g., power electronics in aircraft [1], modern rectifier systems have to meet high requirements concerning efficiency, weight, and compactness. Active three-phase rectifiers offer the possibility to comply with rigorous low-frequency current harmonics limits but show a large high-frequency noise level. Passive low-pass filters employing inductors and capacitors in connection with resistors providing passive damping can be used to attenuate resulting conducted emissions (CE) of the systems [2]–[4]. These passive filter elements take up a relatively large portion of overall system volume and can only be reduced in volume by increasing the switching frequency.

It is common and very helpful to split the generated electromagnetic interference (EMI) emissions into a common mode (CM) and differential mode (DM) component. DM noise currents flow in and out through the phases whereas CM currents return via earth. Hence, different filter strategies and filter elements have to be applied to handle the two emission types. As will be shown in Section II, asymmetrical currents to earth caused by asymmetrical impedances of the rectifier system also generate DM noise. These type of emissions are called "nonintrinsic DM noise" [5] or "mixed-mode (MM) noise" and their origin was analyzed in [6] and [7] for single-phase flyback converters. The MM noise in three-phase diode front-end converters was discussed in [8] and [9].

The performance of the DM filter can be well predicted. Dependent upon the required attenuation, multistage *LC*-filters are usually applied [10]. "Zero-ripple" DM filter concepts have also been proposed [11]. On the contrary, CM emissions are mainly determined by parasitic elements such as capacitances of semiconductors to the heat sink, capacitances between heat sink and earth, magnetic couplings of inductors, etc., and are, therefore, difficult to identify and quantify. In [12] and [13], a CM-noise-modeling technique for single-phase power-factor correction (PFC) systems was proposed, which considers the parasitic capacitances of semiconductors to the heat sink. Several works on three-phase systems were also done [14], [15] where some insights in the CM noise sources and propagation paths in three-phase systems are given. These papers, however, only include limited information and guidelines for final EMI filter design. In this paper, the CM noise modeling technique for single PFC [12], [13] will be extended to three-phase systems and an EMI filter design and implementation for an ultracompact three-phase/level PWM rectifier (see Fig. 1 where the parasitic capacitances relevant for $i_{\mathrm{N}1} > 0, i_{\mathrm{N}2}, i_{\mathrm{N}3} < 0$ are shown) [16] will be discussed. In [17], the formation of the CM voltage was analyzed in detail but for the sake of simplicity only a single lumped capacitor from the output voltage midpoint M to earth was used to model the CM current paths. This is a reasonable approach to get an overview of the CM behavior of a system but proved to be insufficiently accurate for designing the EMI filter. Based on the modeling technique, considering parasitic capacitances of the semiconductors to the heat sink and from the output voltage rails to earth a more detailed CM model will be developed in Section II. The resulting EMI filter should show minimum volume in order to achieve the highest possible rectifier power density and for this reason a switching frequency of 1 MHz is chosen [18].

In [17], a concept for minimizing the high-frequency CM emissions was proposed (further concepts can be found in [19]). The output voltage midpoint M is connected to an artificial mains star-point N' formed by capacitors C. The low-frequency

Manuscript received May 6, 2010; revised July 13, 2010; accepted August 10, 2010. Date of current version June 10, 2011. Recommended for publication by Associate Editor P. Tenti.

M. Hartmann and J. W. Kolar are with the Power Electronic Systems Laboratory, ETH Zurich, CH-8092 Zurich, Switzerland (e-mail: hartmann@lem.ee.ethz.ch; kolar@lem.ee.ethz.ch).

H. Ertl is with the Power Electronics Section, Vienna University of Technology, A-1040 Vienna, Austria (e-mail: j.ertl@tuwien.ac.at).

Color versions of one or more of the figures in this paper are available online at http://ieeexplore.ieee.org.

Digital Object Identifier 10.1109/TPEL.2010.2070520

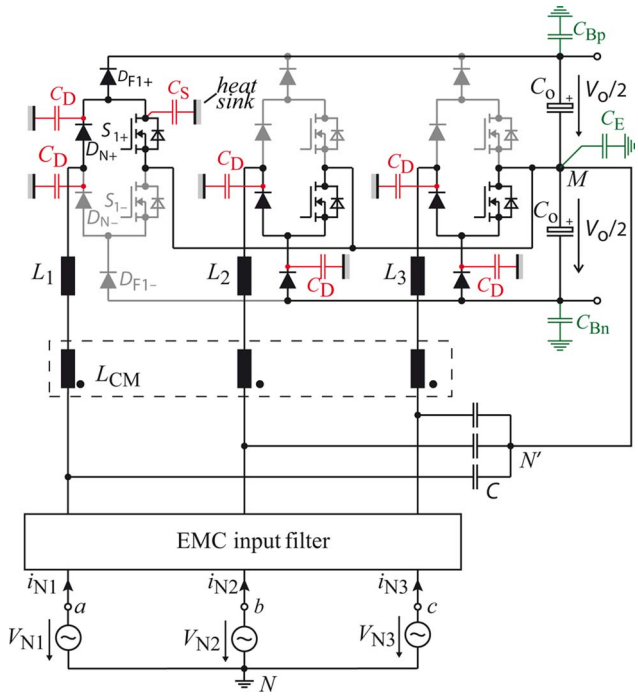

Fig. 1. Schematic of the three-phase/level PWM rectifier including relevant parasitic capacitances from semiconductors to heat sink (C_S and C_D) and from the dc output rails to earth (C_{Bp}, C_{Bn}, and C_{E}) for $i_{\mathrm{N1}} > 0$, $i_{\mathrm{N2}}, i_{\mathrm{N3}} < 0$. In addition, the proposed CM voltage reduction concept is shown, where the output voltage midpoint M is connected to an artificial mains star point N'. High-frequency CM currents are limited by a three-phase CM inductor L_{CM}.

CM voltage used to increase the input voltage range of the rectifier drops across the capacitors C while all high-frequency CM output voltage components are attenuated by the low-pass filter action of the boost inductors L_i and the capacitors C. Unfortunately, this concept results in a considerably increased ripple of the boost inductor currents and/or in higher copper and core losses. Therefore, the basic concept is extended here by placing a three-phase CM inductor L_{CM} in series to the boost inductors L_i, which considerably reduces the additional high-frequency current ripple.

The DM filter design as well as the design of the proposed CM filter inductor will be discussed in Section III where a simplified method for determining the CM noise level is also proposed. Section IV deals with the practical implementation of the filter considering commercially available magnetic materials. Measurements taken from a 10 kW rectifier prototype verify the effectiveness of the proposed EMI filter in Section V. In this section, several practical aspects of filter implementation like the physical component arrangement, shielding layers, and magnetic couplings, etc., are discussed with reference to measurement results.

II. Converter Noise Model

The semiconductors of a power electronics converter are typically mounted on a common heat sink, which is usually connected to earth. Therefore, parasitic capacitances to earth exist although not included in the basic circuit diagram. In order to fully understand the propagation of the resulting CM noise currents, these capacitances have to be considered and/or a detailed CM noise model has to be derived. However, first of all, a review on noise components in three-phase systems will be given.

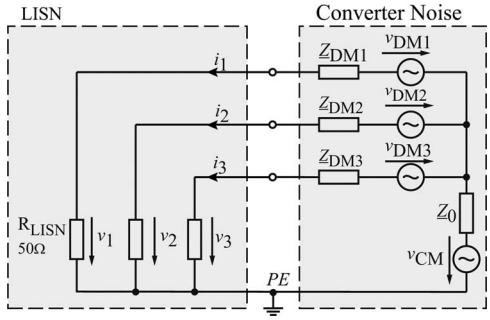

Fig. 2. High-frequency noise model of a three-phase rectifier system connected to a three-phase LISN.

A. Review on Three-Phase Noise Components

Separation of CM and DM noise in three-phase systems is not easily possible. Orthogonal transformations as reported in [20] and [21] can be applied but these transformations, however, are only valid if the three-phase system is symmetrical, linear, and time invariant. Regardless of the intended three-phase system and its noise sources, the CM current can be defined as the current flowing out through the phases and returning via earth. The CM current is, hence, the sum of all three-phase currents

$$i_{\mathrm{CM}} = i_1 + i_2 + i_3 \,. \tag{1}$$

The DM currents, on the other hand, can be defined as the currents flowing out through one phase and returning through the two other phases, which implies $i_{\mathrm{DM},1} + i_{\mathrm{DM},2} + i_{\mathrm{DM},3} = 0$. A general high-frequency noise model of a three-phase system is given in Fig. 2, where the line impedance stabilization network (LISN) is modeled as three 50 Ω resistors. In addition to the DM noise sources $v_{\mathrm{DM,i}}$ and their source impedances $\underline{Z}_{\mathrm{DM,i}}$, the CM noise source v_{CM} is also shown together with a single lumped impedance to earth $\underline{Z}_0$. This model implies that the propagation paths of the DM and CM currents can be separated—which may not be true in every case. If current and voltage signals at the interconnections of the device under test to the LISN are considered, the definition of (1) is still valid even if coupled noise propagation paths exist. The CM voltage at the LISN can be calculated by

$$v_{\mathrm{CM}} = i_{\mathrm{CM}} \frac{R_{\mathrm{LISN}}}{3} = \frac{v_1 + v_2 + v_3}{3} \tag{2}$$

where R_{LISN} is the input resistance of the LISN. By the use of (2), the DM voltage component of phase 1 can be calculated to

$$v_{\mathrm{DM},1} = v_1 - v_{\mathrm{CM}} = \frac{2v_1}{3} - \frac{v_2}{3} - \frac{v_3}{3}. \tag{3}$$

If a symmetrical distribution of the CM current i_{CM} on all three phases is assumed, then each phase current can be written as

$$i_i = i_{\mathrm{DM,i}} + \frac{i_{\mathrm{CM}}}{3}. \tag{4}$$

Note that some authors, e.g. [6], define the CM current as the current common in all three phases ($i_i = i_{\mathrm{DM,i}} + i_{\mathrm{CM}}$), which results in a current to earth of $3i_{\mathrm{CM}}$ instead of i_{CM}. If, unlike in Fig. 2, the impedances of the three phases to earth differ, then the CM current distribution in the three phases is also not equal. Let Δi be the deviation of the CM current in phase 1 to the current i_0 of the two other phases. According to (1), the resulting CM current is given by $i_{\mathrm{CM}} = 3i_0 + \Delta i$. The input currents can, therefore, be written as

$$\begin{aligned} i_1 &= i_{\mathrm{DM},1} + \frac{i_{\mathrm{CM}}}{3} + \frac{2\Delta i}{3} \\ i_2 &= i_{\mathrm{DM},2} + \frac{i_{\mathrm{CM}}}{3} - \frac{\Delta i}{3} \\ i_3 &= i_{\mathrm{DM},3} + \frac{i_{\mathrm{CM}}}{3} - \frac{\Delta i}{3} \end{aligned} \tag{5}$$

which yields to the CM voltage

$$v_{\mathrm{CM}} = R_{\mathrm{LISN}} \left(i_0 + \frac{\Delta i}{3} \right). \tag{6}$$

By subtracting the CM voltages from the according phase voltages $v_{\mathrm{DM,i}} = v_i - v_{\mathrm{CM}}$, the DM voltages result in

$$\begin{aligned} v_{\mathrm{DM,MM},1} &= R_{\mathrm{LISN}} \left(i_{\mathrm{DM},1} + \frac{2\Delta i}{3} \right) \\ v_{\mathrm{DM,MM},2} &= R_{\mathrm{LISN}} \left(i_{\mathrm{DM},2} - \frac{\Delta i}{3} \right) \\ v_{\mathrm{DM,MM},3} &= R_{\mathrm{LISN}} \left(i_{\mathrm{DM},3} - \frac{\Delta i}{3} \right) \end{aligned} \tag{7}$$

which show, in comparison to (3), an additional part caused by the unequal distributed CM currents. Unbalanced CM noise, hence, also causes DM noise and this supplementary DM noise is called "nonintrinsic DM noise" or "MM noise." The applied definition of the CM current offers an explanation of the phenomenon of nonintrinsic DM noise, whereas the model with $i_{\mathrm{Earth}} = 3i_{\mathrm{CM}}$ cannot explain it without introducing an additional noise source.

B. Derivation of Noise Model

In the following, the modeling approach given in [12] and [13] for single-phase PFC will be extended to three-phase systems.

In Fig. 1, the relevant parasitic capacitors between semiconductors and heat sink are drawn for $i_{\mathrm{N1}} > 0$, $i_{\mathrm{N2}}, i_{\mathrm{N3}} < 0$. The capacitors C_S and C_D represent the stray capacitance of a MOSFET's drain and a diode's cathode to the heat sink, which is approximately 60 pF for the applied TO220 package. These capacitances are present for all semiconductors of the rectifier system, but the capacitors which are not carrying current in $-30° < \varphi_{\mathrm{N}} < 30°$ are not shown. The capacitors C_{Bp} and C_{Bn} model the stray capacitances of the positive and negative output voltage rail to earth. The capacitor C_E models the parasitic capacitance of the output voltage midpoint to earth but also includes possible parasitic capacitances of the load. Therefore, the capacitance of C_E can be comparably large, e.g., several nanofarad. In order to develop a high-frequency CM model of the circuit, the MOSFETs are replaced by voltage sources $v_{v,i}$, which impress the switched voltage waveforms. In a similar manner, the diodes D_{F1+}, D_{F2-}, and D_{F3-} are replaced by current sources showing the same pulsed current waveform. The impedance of the output capacitor C_o, implemented partly with ceramic capacitors, is very small at switching frequency (1 MHz), and therefore, modeled as a short circuit. The corresponding mains diodes D_{N+}/D_{N-} are permanently ON during a half mains period and are, hence, also replaced by a short circuit. The resulting equivalent circuit is given in Fig. 3. As the rectifier system is modeled by linear elements, the influence of the noise sources can be analyzed by application of the superposition theorem. In Fig. 4(a), the corresponding noise model is drawn if only current noise sources are considered. It is obvious that the current sources are shorted by the low impedance paths established by the output capacitors and that they do not contribute to the noise measured in the LISN. If only voltage noise sources are considered, then the equivalent circuit given in Fig. 4(b) can be derived.

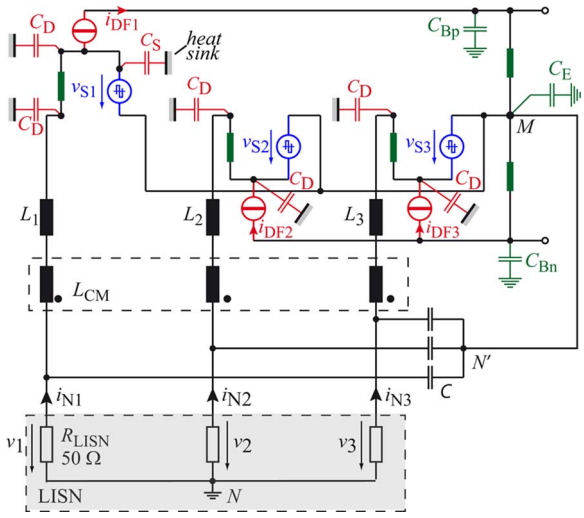

Fig. 3. High-frequency equivalent circuit if the operated switches are replaced by voltage noise sources and the corresponding free-wheeling diodes are replaced by current noise sources. Model is valid for $i_{\mathrm{N1}} > 0$, $i_{\mathrm{N2}}, i_{\mathrm{N3}} < 0$.

The phase leg with positive input current (i_{N1}) shows a total capacitance of $C_p = 2C_D + C_S$ to the heat sink and the phase legs with negative input currents (i_{N2} and i_{N3}) show a total capacitance of $C_n = 2C_D$, which is different to C_p. Note that this model is only valid for $i_{N1} > 0$, $i_{N2}, i_{N3} < 0$, i.e., $-30° < \varphi_N < 30°$, and that the capacitance of C_p and C_n is changing if one of the input phase currents changes sign, i.e., every 60°. The capacitor C_g models all capacitances from the output voltage rails and the output voltage midpoint to earth ($C_g = C_E + C_{\mathrm{Bp}} + C_{\mathrm{Bn}}$). The detailed function of the CM filtering based on a connection of M with N' will be discussed later. Note that the voltage sources $v_{v,i}$ include DM emissions as well as CM emissions. In Fig. 4(b), only current paths involving the parasitic capacitors C_p and C_n are shown.

Different possibilities for defining the heat sink potential exist and the most important ones will be discussed shortly as they result in different CM behavior.

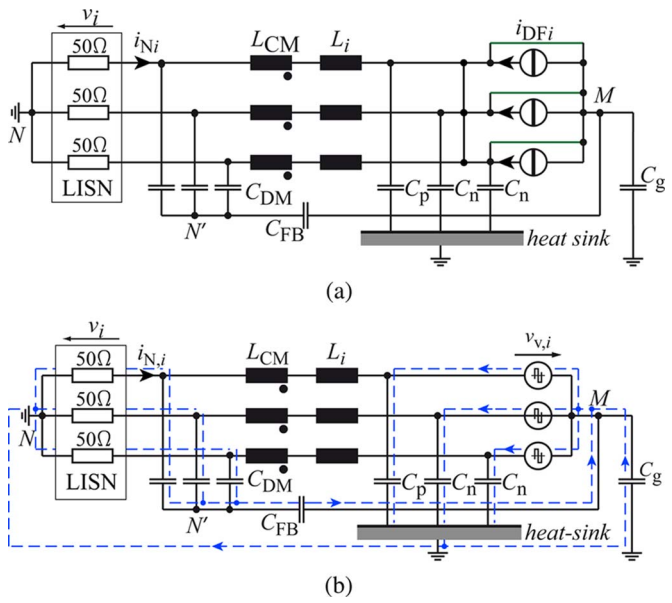

Fig. 4. Detailed noise models valid for $i_{N1} > 0$, $i_{N2}, i_{N3} < 0$, if the heat sink is connected to earth if (a) only current noise sources and (b) only voltage noise sources are considered. In (b), only current paths involving the parasitic capacitors C_p and C_n are shown.

1) Heat Sink Connected to the Output Voltage Midpoint M: If the heat sink is connected to M, C_p, and C_n lie in parallel to the voltage sources. The noise currents through them are guided directly back to the noise source and, thus, no additional external CM noise occurs. This is the best option from the EMI perspective but one must keep in mind that M will show a low-frequency CM voltage of a few 100 V if a third harmonic injection signal is applied and this may, depending on the application, not be permitted.

2) Heat Sink Connected to Earth: In many applications, the heat sink has to be connected to earth due to safety reasons. The largest impact on the noise emissions can then be observed. According to Fig. 4(b), the three phases show different capacitances to earth and, therefore, a separation into CM and DM equivalent circuits is not directly possible. These unequal impedances to earth result in an unbalanced CM current distribution of the three phases, which finally yield to nonintrinsic DM emissions as shown in Section II-A. These nonintrinsic DM emissions are not analyzed further in this paper but are subject to further research on this topic. However, if the parasitic capacitors are assumed to be equal, then an equivalent circuit with separated CM and DM emissions can be drawn. This will be further discussed in Section III.

3) Heat Sink Floating: If the heat sink is floating, then one must deal with a similar situation to where the heat sink is connected to earth. The heat sink would show a parasitic capacitance to earth of a few picofarad, which is now connected in series to the capacitances C_p and C_n. As this parasitic capacitance is typically much smaller than C_p and C_n, the resulting total capacitances to earth are almost equal and an equivalent circuit with separated CM and DM emissions can be drawn.

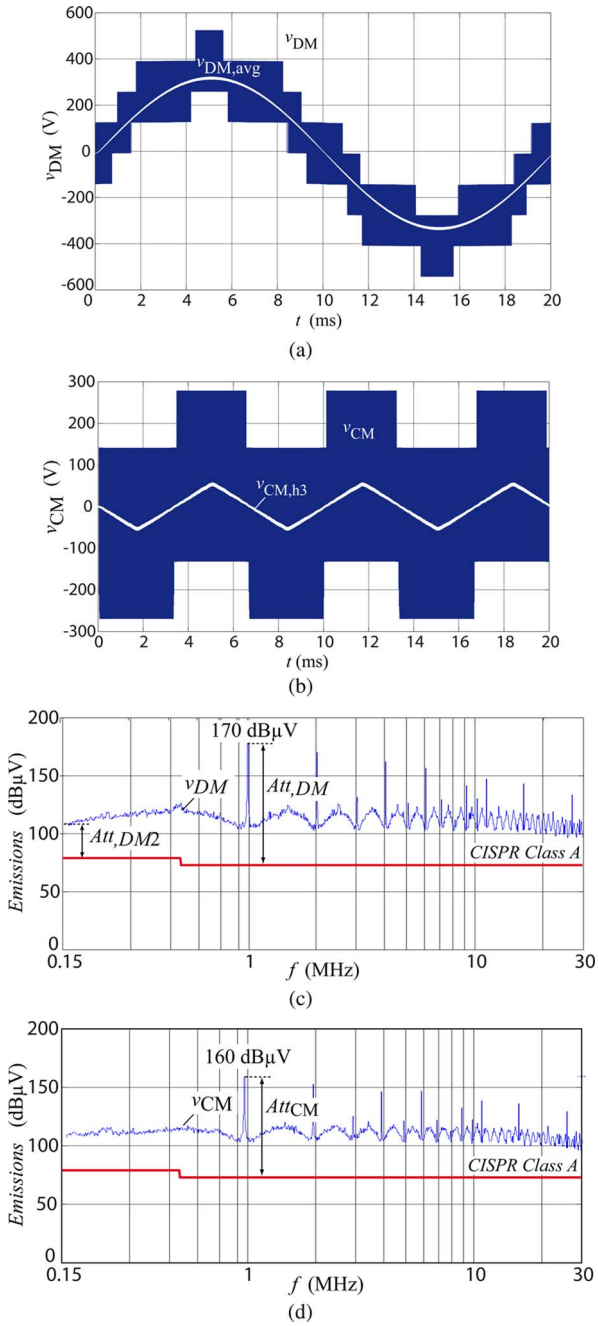

Fig. 5. Simulated voltage waveforms of the rectifier system operated at an output power of $P_o = 10\,\mathrm{kW}$ and corresponding predicted spectra using peak-detection. (a) DM voltage, (b) CM voltage, (c) predicted DM emission, and (d) predicted CM emission.

III. Filter Design

In order to design a proper EMI filter, the CM and DM noise levels of the three-phase rectifier system are required. A computer simulation is used to determine the DM and CM voltage waveforms [see Fig. 5(a) and (b)] generated by the rectifier system. The assumed system specifications are listed in Table I. It has to be stated here that different modulation strategies result in different CM and DM voltage waveforms, which would finally lead to different EMI filter requirements. In three-phase PWM

TABLE I
SPECIFICATIONS OF THE ANALYZED PWM RECTIFIER SYSTEM

V_{Ni}	230 V
f_N	50/60 Hz
f_s	1 MHz
V_o	800 V_{DC}
P_o	10 kW

rectifier systems, a third harmonic signal is added to the sinusoidal phase-voltage reference values in order to increase the input voltage modulation range for a given output dc voltage. A triangular shaped signal

$$v_{h3} = \frac{\hat{V}_N}{6}\mathrm{tri}(3\varphi) \tag{8}$$

is employed in the implemented modulator, which results in a triangular low-frequency component ($v_{CM,h3}$) of the CM voltage [see Fig. 5(b)].

According to the calculation scheme given in [10], the Quasi-Peak or Peak weighted DM and CM spectrum can be calculated. The calculated spectra (using peak-detection) of the voltages shown in Fig. 5(a) and (b) are depicted in Fig. 5(c) and (d), together with the limit defined by CISPR11 class A [22]. The results of this calculation are only the spectra of the simulated voltage waveforms and, contrary to [10], the influence of the LISN is not considered. The EMI filter must now be designed such that the generated emissions do not exceed the CISPR11 class A. The influence of the LISN has to be considered later in the EMI filter design process.

According to Fig. 5, the main amplitudes of harmonics occur at multiples of the switching frequency. Hence, the required attenuation of the DM and CM filters can be calculated by comparing the simulated emissions with the limit specified in CISPR11. For the DM filter this results in a required attenuation of

$$\begin{aligned}\mathrm{Att_{DM}[dB]} = {} & v_{\mathrm{DM}}(f_s)[\mathrm{dB}\mu\mathrm{V}] - \mathrm{Limit}[\mathrm{dB}\mu\mathrm{V}] \\ & + \mathrm{margin[dB]} \cong 103\,\mathrm{dB}\end{aligned} \tag{9}$$

where a margin of 6 dB is included. The required attenuation of the CM filter can be calculated as

$$\begin{aligned}\mathrm{Att_{CM}[dB]} = {} & v_{\mathrm{CM}}(f_s)[\mathrm{dB}\mu\mathrm{V}] - \mathrm{Limit}[\mathrm{dB}\mu\mathrm{V}] \\ & + \mathrm{margin[dB]} \cong 93\,\mathrm{dB}.\end{aligned} \tag{10}$$

The process employed for calculating the noise spectra is a time-consuming task. The results of this calculation are noise amplitudes over the whole frequency range but, as shown earlier only the amplitude of the emissions generated at the switching frequency fundamental is used for EMI filter design (in case of $f_s \geq 150$ kHz). In [23], an approximation method for determining the EMI emission has been presented, where only the fundamental DM component at the switching frequency is considered. However, this method can also be applied to determine the CM filter requirements. Therefore, the rms value of the CM voltage $V_{CM,rms}$, which comprises a low-frequency component $V_{CM,h3,rms}$ and a high-frequency component $V_{CM,noise,rms}$ containing all switching frequency harmonics must be calculated. This could be done purely analytically but for the sake of simplicity the rms value of the total CM voltage is calculated using the simulated CM voltage shown in Fig. 5(b). The rms value of the high-frequency CM noise $V_{CM,noise,rms}$ is, therefore, given as

$$V^2_{\mathrm{CM,noise,rms}} = V^2_{\mathrm{CM,rms}} - V^2_{\mathrm{CM,h3,rms}}\,. \tag{11}$$

Substituting (8) in (11) yields

$$V^2_{\mathrm{CM,noise,rms}} = V^2_{\mathrm{CM,rms}} - \frac{\left(\hat{V}_N/6\right)^2}{3} \tag{12}$$

which results in an estimated noise level of

$$V_{\mathrm{CM,noise}} = 164\,\mathrm{dB}\mu\mathrm{V}. \tag{13}$$

The difference to the result given in Fig. 5(d) is only $4\,dB\mu V$, and therefore, the proposed procedure is a very simple method to estimate the EMI filter requirements.

According to Fig. 5(c) and (d), a relatively large noise floor of ≈ 110 dB is generated by the rectifier system. The reason for this can be found in the time behavior of the DM and CM voltages. As reported in [24]–[26], the carrier sideband harmonics are present in the spectrum of the PWM signal with low-frequency local average. This leads to an increased noise floor, which has to be considered in the DM filter design. Therefore, the DM filter has to reach an attenuation of at least

$$\begin{aligned}\mathrm{Att_{DM2}[dB]} = {} & v_{\mathrm{DM}}(150\,\mathrm{kHz})[\mathrm{dB}\mu\mathrm{V}] - \mathrm{Limit}[\mathrm{dB}\mu\mathrm{V}] \\ & + \mathrm{margin[dB]} \cong 37\,\mathrm{dB}\end{aligned} \tag{14}$$

at the lower frequency limit for CE measurements, i.e., at 150 kHz. At least, one filter stage has to be designed such that the required attenuation at [150]kHz is reached. This means the volume of this filter stage cannot be reduced by a high-switching frequency. Among other limitations, such as the lack of available high-frequency magnetic materials, this is a main limitation of EMI filter volume reduction by increasing the switching frequency.

A. DM Filter Design

In addition to the required filter attenuation for DM filter design, the phase displacement of the mains currents resulting from the currents drawn by the filter capacitors must also be considered. If a maximum phase displacement should be limited to 10° at an output power of $0.1\,P_o$, then the DM filter capacitors here are limited to a total capacitance of $C_{\mathrm{DM}} = 3.5\,\mu\mathrm{F}$ per phase. According to the specifications given in (9) and (14), an *LC*-filter with three stages is used for construction of the DM filter. The single-phase equivalent circuit of the DM filter is shown in Fig. 6(a). The boost inductor of the rectifier can be used to realize the first filter stage. The inductance value of the boost inductor is defined by the maximum allowed current ripple. A maximum current ripple of $\Delta i_{\mathrm{L,pp}} = 0.2\,\hat{I}_{\mathrm{N,i}}$ shall be allowed for the implementation at hand, which results in an inductance of $L_i = 20\,\mu\mathrm{H}$. In [27], it was shown that a maximum attenuation for a multistage *LC*-filter can be achieved if all inductance

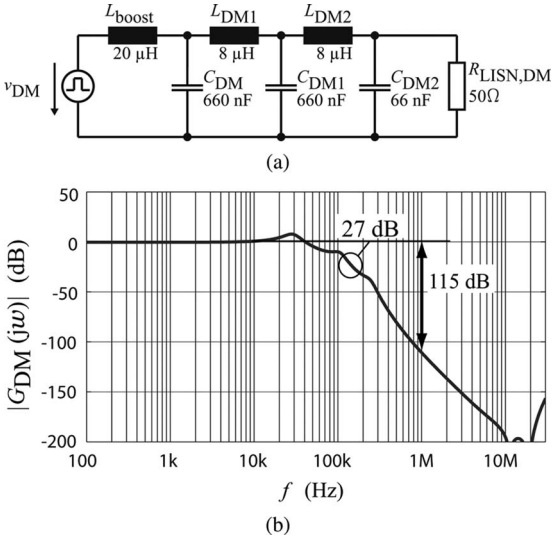

Fig. 6. (a) Equivalent single-phase DM model and (b) calculated transfer function $G_{\text{DM}}(\text{j}\omega)$of the designed DM filter.

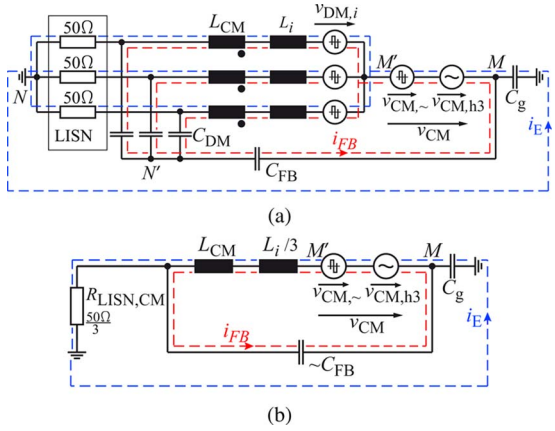

Fig. 7. (a) Conducted noise equivalent circuit of the three-phase/level PWM rectifier system for the proposed CM filter concept if Cp and C_n are neglected and (b) simplified CM equivalent circuit.

values and all capacitance values are equal, which also implies that the cut-off frequencies of all filter stages are identical. Unfortunately, (9) as well as (14) must be satisfied, something that is not possible with regard to a minimum filter volume by application of this criteria. In addition, this concept shows the problem of multiple equal filter resonance frequencies. Hence, the cut-off frequencies of the filter stages are selected in a distributed manner and the resulting filter components are chosen also considering aspects of practical construction. This will be discussed further in Section IV. The calculated transfer function $G_{\text{DM}}(\text{j}\omega)$ of the designed filter is depicted in Fig. 6(b).

B. CM Filter Design

In a first step design of the CM filter, the influence of the parasitic capacitors C_p and C_n (see Fig. 4) is neglected. Safety regulations must be considered in the selection of CM capacitors where the leakage earth current is limited to several milliampere. This results in a limited total capacitance connected to earth, which fundamentally influences CM filter design. If a conventional multistage *LC* low-pass filter would be implemented, then at least three stages would be necessary while the large CM component of V_o would still be present. However, by connecting the output voltage midpoint M to an artificial star-point N' as shown in Fig. 1, the CM component of the output voltage can be reduced significantly without violating the safety regulations. The capacitors C_{DM} of the first DM filter stage can be advantageously used to form N'. An equivalent circuit of the proposed CM filter concept is shown in Fig. 7(a). There, the converter voltage $v_{v,i}$ is split into a DM voltage $v_{\text{DM,i}}$ and a CM voltage v_{CM}

$$v_{v,i} = v_{\text{DM,i}} + v_{\text{CM}} \tag{15}$$

where the CM voltage

$$v_{\text{CM}} = v_{\text{CM},\sim} + v_{\text{CM,h3}} \tag{16}$$

comprises a high-frequency component $v_{\text{CM},\sim}$ and a low-frequency component $v_{\text{CM,h3}}$, which represents the third-harmonic injection mentioned earlier. The CM filter path is implemented by a capacitor C_{FB} in series to the DM capacitors forming N'. In addition, the capacitance C_g representing the lumped capacitance between M and earth is shown. It is significantly influenced by the load. If this parasitic capacitance is neglected for a first analysis, the generated CM voltage appears across circuit L_i, L_{CM}, and the series connection of the capacitors C_{FB} and C_{DM}. The capacitors C_{FB} and C_{DM} are not connected to earth and are, therefore, not limited in capacitance by equipment safety regulations. The construction of a CM inductor, which is able to handle the third-harmonic voltage component $v_{\text{CM,h3}}$ without saturation is possible but would result in a very large and bulky element. If the feedback capacitor C_{FB} is dimensioned such that it represents a short circuit for the high-frequency CM signals ($v_{\text{CM},\sim}$) but a high impedance element for the third-harmonic component ($v_{\text{CM,h3}}$), the low-frequency component will drop across the feedback capacitor and only $v_{\text{CM},\sim}$ has to be handled by the inductors. Unfortunately, three-phase CM inductors typically allow only a very small zero-sequence current without saturation because of their very high permeability. Due to

$$i_{\text{FB,h3}} \approx C\frac{dv_{\text{CM,h3}}}{dt} \tag{17}$$

the feedback capacitor has to be as small as possible to prevent saturation of the CM inductor. Hence, the relatively large DM capacitors C_{DM} (660 nF per phase) cannot be used alone for implementation and a low-capacitance feedback capacitor C_{FB} is connected in series to the star-point N'.

The CM inductor, on the other hand, has to hold the high-frequency CM voltage and core saturation is avoided if

$$B_{\text{sat}} > B_{\text{CM,max}} = \frac{\int_0^{T_{\text{p}}} v_{\text{CM},\sim}dt}{N\,A_{\text{fe}}} = \frac{(V_o/3)T_s}{N\,A_{\text{fe}}} \tag{18}$$

where $T_s = 1/f_s$ and T_p denotes the maximal length of a CM pulse, which was set to $T_p = T_s$.

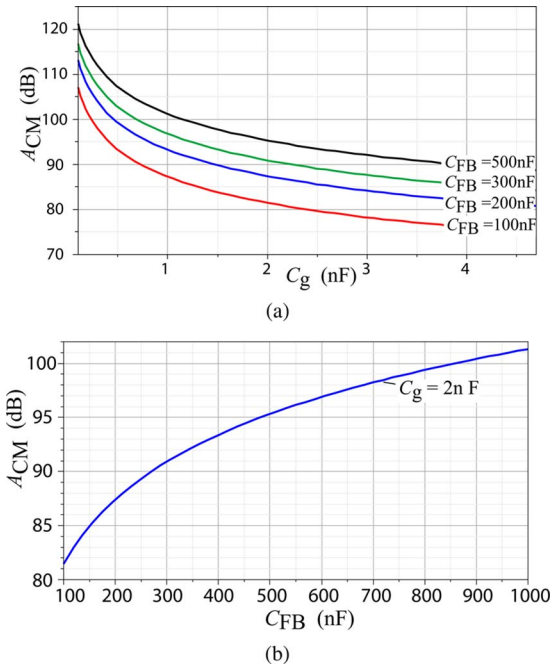

Fig. 8. (a) Attenuation A_{CM} of the proposed CM filter concept as a function of earth capacitance C_g and (b) achieved attenuation as a function of C_{FB} for $C_g = 2\,\mathrm{nF}$ ($f = 1$ MHz).

As the CM inductors are placed in series to the boost inductors L_i the full-phase current including the high-frequency ripple flows through their windings. The high-frequency DM current ripple does not cause core losses due to the mutual compensation of the magnetomotive forces but copper losses caused by skin and proximity effect have to be considered.

In Fig. 7(b), the CM equivalent circuit is shown. If the lumped capacitance C_g is not neglected, part of the total CM current does not return through the feedback path i_{FB}. Depending on the size of C_g, this results in a notable earth current through LISN. In order to limit this current, the feedback capacitor should be large which is, however, in contradiction to the design criteria given in (17). Depending on the parasitic capacitances C_g and C_{FB}, the attenuation A_{CM} can be calculated by

$$A_{\mathrm{CM}} = 20\,\log_{10}\left(\left|\frac{1 + A\,s + \underline{Z}_L\,C_g\,C_{\mathrm{FB}}\,R_{\mathrm{LISN,CM}}\,s^2}{R_{\mathrm{LISN,CM}}\,C_g\,s}\right|\right)$$

$$A = C_g\,(\underline{Z}_L + R_{\mathrm{LISN,CM}}) + \underline{Z}_L\,C_{\mathrm{FB}} \qquad (19)$$

where $\underline{Z}_L$ denotes the total impedance of the CM inductor and $R_{\mathrm{LISN,CM}}$ is the equivalent high-frequency CM LISN impedance ($R_{\mathrm{LISN,CM}} = 16.7\,\Omega$). In Fig. 8(a), the resulting attenuation of the constructed filter is plotted as a function of the earth capacitance C_g. It is obvious that the required attenuation of 93 dB can only be achieved with the proposed concept if either $C_{\mathrm{FB}} > 500\,\mathrm{nF}$ or $C_g < 1\,\mathrm{nF}$. A higher amount of capacitance to earth would result in an attenuation lower than the required value given in (10). According to Fig. 8(b), a higher capacitance of C_{FB} would increase the attenuation but this would also increase the low-frequency current $i_{\mathrm{CM,h3}}$ and is, therefore, not an option. A compromise of $C_{\mathrm{FB}} = 200\,\mathrm{nF}$ is used for the filter presented in this paper. As a result, an additional CM filter stage, which must attain the missing attenuation of ≈ 20 dB, is required.

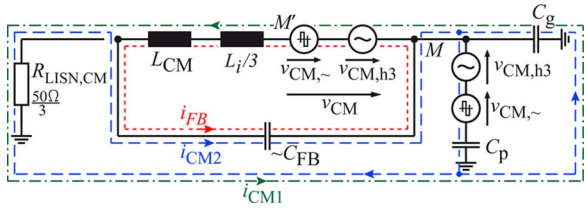

Fig. 9. CM equivalent circuit of the three-phase/level PWM rectifier with heat sink connected to earth if C_p and C_n are assumed to be equal.

Until this point, the capacitors C_p and C_n of the extended noise model given in Fig. 4 have been neglected for CM filter design. According to (15), the total converter noise $v_{\mathrm{v,i}}$ can be divided into DM and CM emissions, if the two lumped parasitic capacitors are assumed to be equal ($C_p = C_n$). Hence, a simplified CM model can be drawn, which is shown in Fig. 9. It is obvious that even if the proposed CM concept operates ideally ($i_{\mathrm{CM1}} = 0$), a CM current i_{CM2} through the LISN exists (marked as a blue dashed line). This current is caused by the parasitic capacitances of the semiconductors to the heat sink (if the heat sink is connected to earth) and can only be reduced by insertion of an additional CM filter stage. As already discussed, this additional filter stage is needed in any case in order to achieve the required attenuation given in (10). It has to be stated here that the proposed CM filter concept (connection of M with N') supports the propagation of this type of CM emissions and that a large capacitance C_g would help to reduce the emissions. However, the advantage of an output voltage without high-frequency CM component clearly dominates this drawback.

IV. Filter Construction

Having determined the EMI filter topology and calculation of the filter performance, the implementation of the passive components is an important design step. A proper magnetic material has to be chosen for implementation of the inductors. In Fig. 10(a), the complex permeability $\mu = \mu' - \mathrm{j}\mu''$ of the widely used ferrite materials N97 and N49 from EPCOS Inc. are plotted. According to Fig. 10(a), the real part of the permeability μ' of material N97 is only constant up to ≈ 1 MHz and drops quickly for higher frequencies. In addition, the imaginary part μ'', which is related to core losses, rises steeply. As a consequence, the material N97 cannot be applied for constructing the boost inductor and is also not a good option for DM filter inductor construction. An implementation using material N49 would be possible for $f_s = 1$ MHz but unfortunately, no suitable core size is commercially available. The permeability of the powder core material -8 from Micrometals Inc. stays constant up to 100 MHz [see Fig. 10(b)] and shows acceptable losses, and is, therefore, used for implementation of the DM and boost inductors. Single layer winding toroids T90-8 with $N = 16$ turns are used for realizing the DM inductors with very small parasitic capacitance. This results in a high self-resonance frequency of 25.9 MHz. Three 220 nF/630V X7R ceramic capacitors in parallel are used for the construction of the DM capacitors C_{DM1}

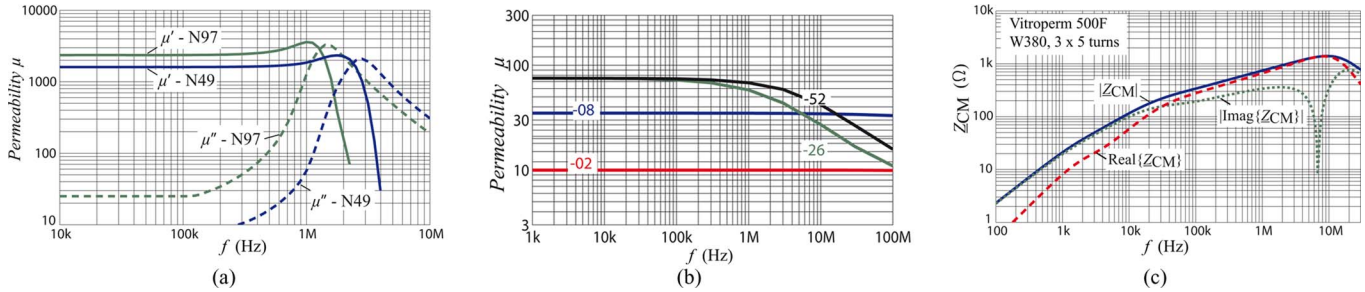

Fig. 10. Real and imaginary part of complex permeability $\mu = \mu' - \mathrm{j}\mu''$ for (a) ferrite materials N97 and N49 of EPCOS, (b) initial permeability for powder core materials from Micrometals, and (c) measured impedance of the constructed three-phase CM inductor ($N = 5\,\mathrm{turns}$) employing Vitroperm 500F from VAC.

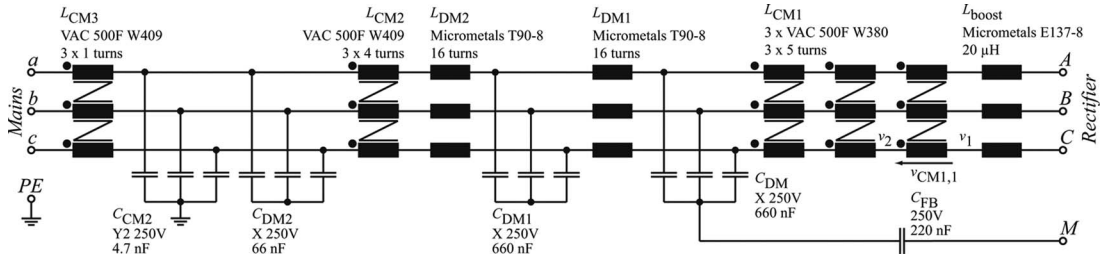

Fig. 11. Complete schematic of the implemented EMI filter including information on the used materials.

and C_{DM2}. Unfortunately, the capacitance of these ceramic capacitors is greatly dependent on the applied voltage, which results in a much smaller effective capacitance. Hence, for the implementation at hand five capacitors must be used. This can be avoided by application of foil capacitors although this results in a greater volume.

The nanocrystalline material Vitroperm 500F of Vacuumschmelze Inc. is used to make the CM inductors. The measured complex insertion impedance $\underline{Z}_{\mathrm{CM}}$ of the CM inductor is plotted in Fig. 10(c). It can be seen that the inductor exhibits a substantial real part of $\underline{Z}_{\mathrm{CM}}$ at $f = 1\,\mathrm{MHz}$, which has to be considered for the design of the CM filter stage. As the material Vitroperm 500F is not typically applied in the frequency range of several 100 kHz, the manufacturer delivers no core loss information for these frequencies. Hence, the core losses of the Vitroperm 500F material at 1 MHz have been measured in the laboratory resulting in the Steinmetz equations

$$P_{\mathrm{VP500F}} = K_c f^{\alpha} B^{\beta} = 44.66 \cdot 10^{-6}[\mathrm{W/dm^3}]\, f^{1.56} B^{1.77} \tag{20}$$

where the frequency f must be in Hertz and the peak flux-density B must be in Tesla. Note that these parameters (K_c, α, β) are only valid for frequencies in the vicinity of 1 MHz. Due to the relative large loss density at 1 MHz three inductors are connected in series for implementation of L_{CM1} in order to limit the core losses. By use of (20), the resulting core losses of each Vitroperm 500F core (W380) can be calculated to $P_{\mathrm{Fe}} = 3.7\,\mathrm{W}$. In order to limit the temperature raise of the CM and boost inductors' small fans are placed between them (see Fig. 11).

The core W409 (also utilizing Vitroperm 500F) is used for the second CM filter stage in conjunction with [4.7]nF Y2-rated ceramic capacitors, which show a very small volume.

The complete schematic of the built filter including detailed information on the materials used is given in Fig. 11. The impedance mismatch concept described in [28] is used for arrangement of the different filter stages. According to this concept, the impedance of the last DM filter stage (C_{DM2}) should be much smaller than the impedance of the LISN ($R_{\mathrm{LISN,DM}} = 50\,\Omega$), which is given for the arrangement shown in Fig. 11. This should also be considered for the last CM filter stage (C_{CM2}). However, the LISN shows a reduced CM impedance $R_{\mathrm{LISN,CM}} = 16.7\,\Omega$ and, in addition, the impedance reduction of the last CM filter stage is limited by equipment safety regulation (C_{CM2}). An additional CM inductor (L_{CM3}) is, therefore, needed to fulfil the impedance mismatch constraint. This CM inductor uses a ferrite core, which is clamped to the power cable. The CM inductors are placed in series to the DM inductors because the stray inductance of the CM inductors then can be used advantageously to increase the DM attenuation.

The constructed EMI filter prototype is shown in Fig. 12(a) together with a picture of the 10 kW laboratory prototype of the rectifier [see Fig. 12(b)]. The overall dimensions of the EMI filter board are 124.5 mm× 110 mm× 33 mm, which results in a power density of 22.1 kW/dm^3 for the EMI filter. The overall rectifier system with the dimensions 195 mm× 110 mm× 33 mm shows a power density of 14.1 kW/dm^3.

The components used in the 10 kW prototype system are listed in Table II. All semiconductors employ the TO220 package. Because of the applied switching frequency of 1 MHz, the system losses are dominated by switching losses. In order

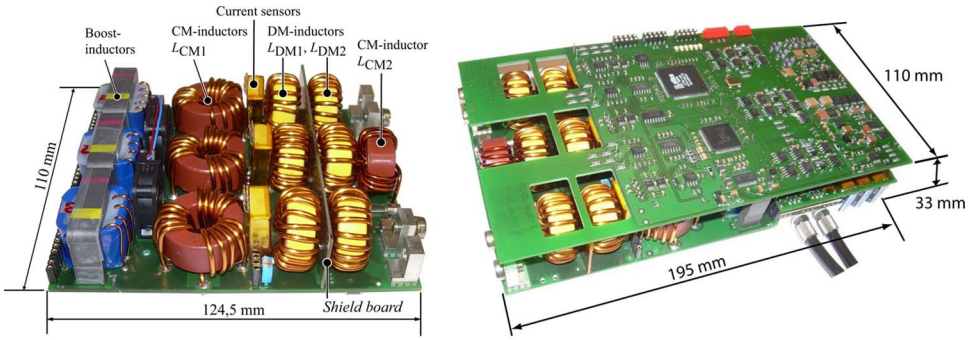

(a) (b)

Fig. 12. (a) Constructed prototype of EMI filter and (b) 10 kW laboratory prototype of the ultracompact rectifier system with a switching frequency of 1 MHz.

TABLE II
COMPONENTS USED IN THE LABORATORY PROTOTYPE SYSTEM

Switches $S_{i,x}$	CoolMOS **IPP60R099CP**, $V_{BRR} = 650\,V$
Free wheeling diodes $D_{iF,x}$	SiC Schottky diode **IDT10S60C**, $V_{RRM} = 600\,V$
Mains diodes D_{iN}	Si rectifier diode **10ETS08**, $V_{RR} = 800\,V$
Start-up thyristors Thy_i	Thyristor **TYN825**, $V_{RR} = 800\,V$
Boost inductors L_{boost}	$20\,\mu H$, Micrometals -8
Output capacitors C_{op}, C_{on}	Partly implemented by ceramic capacitors $92\,\mu F$

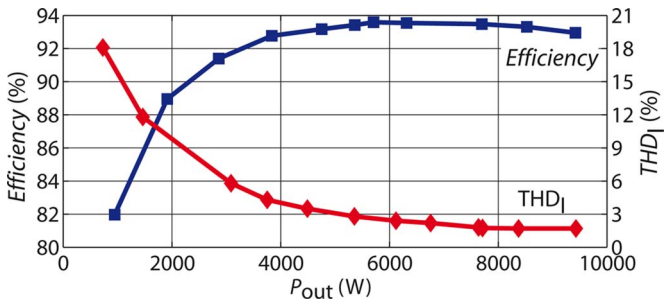

Fig. 13. Measured efficiency and input current quality of the constructed 10 kW rectifier system.

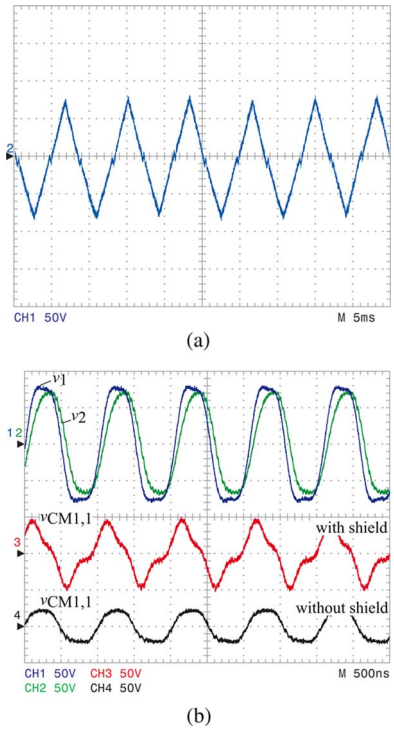

(a) (b)

Fig. 14. (a) Measured CM output voltage component form (from M to earth) employing the proposed CM filter concept and (b) measured voltage of CM inductor $L_{CM1,1}$ with and without PCB shield layer connected to M.

to limit the semiconductor power losses, the CoolMOS device IPP60R099CP in combination with the SiC diode IDT10S60 is used. The SiC diode shows no reverse recovery current I_{rr} but a displacement current is charging the voltage dependent junction capacitance $C_{j,D}$ of the diode. The switching speed of the CoolMOS switches additionally is limited because of a strong voltage and current ringing caused by parasitic elements of the semiconductor devices and the wiring. More details about this limitation can be found in [29]. These effects finally yield to high-switching losses and, hence, only a moderate efficiency slightly below 94% can be achieved (see Fig. 13). On the other hand, the rectifier system still shows a very good input current quality (THDI $< 2\%$ at $P_o = 10\,kW$). The measured THD$_I$ of the input current quality as a function of the output power P_o is also depicted in Fig. 13.

In order to be able to handle the high-frequency ripple current in the output capacitors, ceramic-type capacitors are used in conjunction with electrolytic capacitors for implementation of C_{op} and C_{on}.

V. EXPERIMENTAL RESULTS

Fig. 14 (a) shows the voltage of the output midpoint M against earth. No high-frequency CM voltage is present and only the third-harmonic triangular signal $v_{CM,h3}$, used for increasing the rectifier modulation range is measured. This verifies the proper operation of the proposed CM filter concept. Deviations from the triangular signal can be observed at the zero-crossings where the CM chokes are able to hold the total CM voltage v_{CM} without

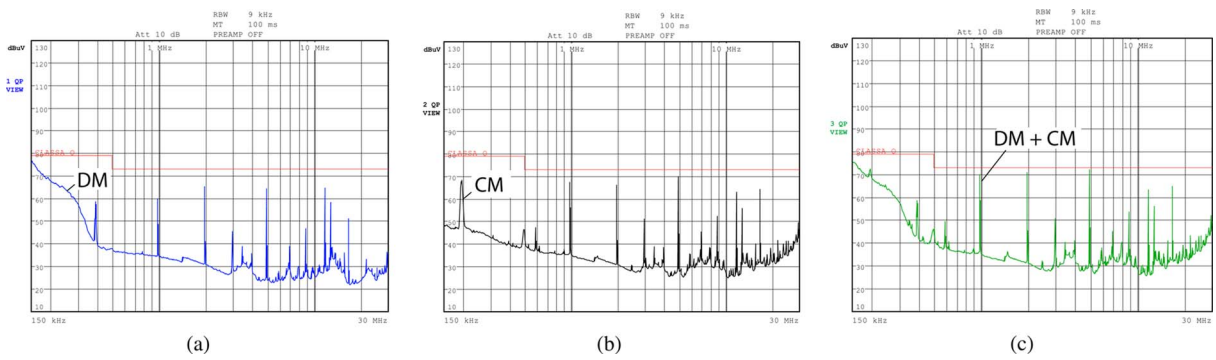

Fig. 15. Final CE measurements of the rectifier system as constructed: (a) DM emissions, (b) CM emissions and (c) total CE.

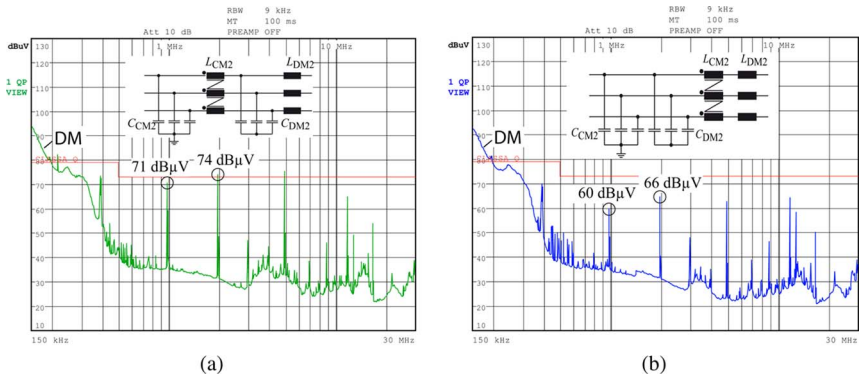

Fig. 16. (a) Measured DM emissions if the CM filter stage arrangement violates the impedance mismatch criteria for the DM filter stage and (b) measured DM emissions if filter satisfies the impedance mismatch criteria.

saturation and the voltage stays zero. After reaching light saturation C_{FB} is charged and the system operates as intended.

In Fig. 15, the results of an EMI measurement according to CISPR 11 (frequency range 150 kHz–30 MHz) are shown together with the limits of CISPR 11 class A. A three-phase DM/CM noise separator was applied to measure the DM and CM noises separately [30]. As expected, the main peaks in the spectra occur at f_s and $2f_s$ and are well below the limit. The peak at 5 MHz results from a shielding layer in the printed circuit board (PCB) and will be discussed later. The peak in the DM spectrum at 400 kHz has its source in the auxiliary power supply and the peak of the CM emissions at 200 kHz is caused by the auxiliary supplies of the gate drives.

Next, the influence of the arrangement of the first DM and CM filter stages (impedance mismatch) is examined. The DM filter capacitors C_{DM2} are moved behind the CM choke L_{CM2} [see Fig. 16(a)] for this purpose. As nothing is changed for the CM path the three Y2-capacitors (4.7 nF) now constitute an additional DM filter stage with the leakage inductance of the CM choke. Unfortunately, the impedance of the Y2-capacitors $|Z_{C,CM2}|_{1\,\mathrm{MHz}} = 1/\omega C_{\mathrm{CM2}} = 33.8\,\Omega$ is in the same range as the DM impedance of the LISN ($R_{\mathrm{LISN,DM}} = 50\,\Omega$) and does not fulfil the impedance mismatch criteria. This results in 10 dB higher noise level compared to an implementation satisfying the impedance mismatch criteria [see Fig. 16(b)]. Therefore, the arrangement of filter stages must be handled with care in order to achieve the desired attenuation.

A. *Parasitic Coupling*

In a practical filter implementation, parasitic magnetic and capacitive couplings between filter elements exist. Since the impact of capacitive coupling is more pronounced at the higher frequencies, one has to be aware that inductive couplings can also cause problems in the frequency range of several kilohertz. Because of these two effects, parasitic coupling between the different filter stages of the multistage filter and also between the three phases occur, which typically degrade the actual filter performance. There has been some research going on in this area and some interesting results can be found in [33]–[35]. The influence of parasitic couplings of the EMI filter at hand is subject for further research but, some effects will be discussed shortly in the the following. It has to be stated here that typical filter elements (capacitors and magnetic materials used for construction of the inductors) usually show component variations of 10% and more and that these component variations might show a higher sensitivity on filter performance than parasitic couplings if a proper PCB layout is done. Parasitic capacitances between traces in the PCB layout are typically in the range of some 10 pF and, hence, may show a more pronounced influence than coupling through air. Also, relatively large magnetic coupling loops may be generated by the traces on the PCB. This highlights that a proper PCB layout is very important to achieve the desired filter performance.

Fig. 17 shows the arrangement of the EMI filter stages. The specific inductors are mounted on the top side of the PCB and the

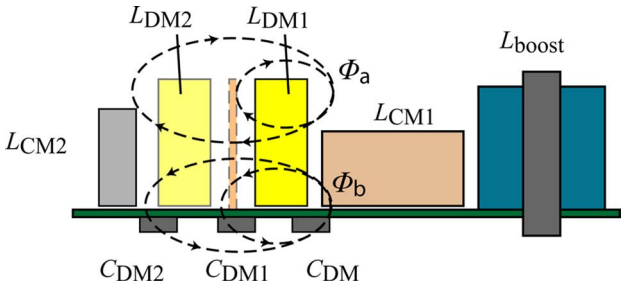

Fig. 17. Arrangement of the EMI filter and inductive coupling caused by the leakage of DM-inductor L_{DM1}.

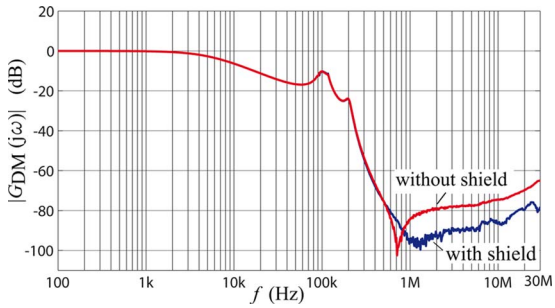

Fig. 18. Measured transfer function $G_{\mathrm{DM}}(\mathrm{j}\omega)$ of the DM filter with and without shield board.

SMD-type ceramic capacitors are soldered on the bottom side of the PCB. The standard toroid winding configuration of the DM inductors presents a large loop area (equivalent to a single turn), which creates a leakage flux (shown for L_{DM1} in Fig. 17). As shown in [33], the magnetic coupling between the stray field of the inductors and filter capacitors could significantly degrade the filter performance for frequencies beyond a few megahertz if foil capacitors are used. At the realization at hand, ceramic capacitors are used for filter implementation, which show a much smaller coupling area than foil capacitors. No pronounced filter degradation caused by this parasitic magnetic coupling is, therefore, expected but this is subject for further research.

As can be seen in Fig. 12(a), the DM inductors C_{DM1} and C_{DM2} are arranged face to face. The implemented winding configuration of these inductors presents a large loop area, which presents a large magnetic coupling to other components. Due to the magnetic coupling of L_{DM1} and L_{DM2}, the attenuation of the DM filter stage is reduced. This coupling could be minimized by a proper arrangement of the DM inductors but this is not an option for the implementation at hand because of the objective of a very high-power density. Another possibility would be to reduce the coupling area of the DM inductors by a winding technique shown in [28]. This winding technique is, however, more expensive and difficult to perform due to the small core geometries in conjunction with the relative large diameter of the solid copper wire ($d = 1.8\,mm$). Instead, a magnetic shield board (0.1-mm-thick Mu-metal foil glued on a PCB with solid copper layer) is inserted between the two stages to reduce the coupling [see Fig. 12(a)]. In Fig. 18, the measured transfer function $G_{\mathrm{DM}}(\mathrm{j}\omega)$ of the filter with and without the shield board is plotted. However, for frequencies below 800 kHz no difference occurs, an improvement of $\approx 10\,\mathrm{dB}$ can be measured for frequencies above 1 MHz. It has to be stated here that the dynamic range of the used network analyzer Bode100 [31] is 100 dB and that the measurement results are, therefore, limited to this value.

In the following, the question if a solid copper layer in the PCB covering the whole power and EMI arrangement as shown in Fig. 19(a) could act as an advantageous shielding layer is discussed. The intention is to connect this copper layer to M in order to catch high-frequency noise currents similar to the proposed CM filter concept. This shield layer, unfortunately, also introduces a (capacitive) coupling path from the interconnections of the three CM chokes forming L_{CM1} to M (see Fig. 11). Due to these capacitive couplings, a uniform voltage distribution between the three CM chokes is inhibited. According to the measurement given in Fig. 14(b), a phase shift of the voltage v_2 (after the first CM inductor $L_{\mathrm{CM1,1}}$) drives this inductor into saturation ($v_{\mathrm{CM1,1}}$ with shield). However, if the shielding layer is not connected to M, then a uniform voltage distribution occurs, which can be verified by the measured voltage ($v_{\mathrm{CM1,1}}$ without shield) whose amplitude corresponds to $v_{\mathrm{CM},\sim}/3$.

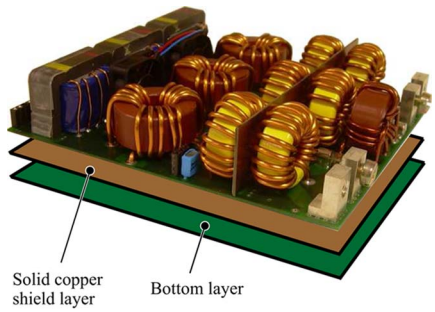

(a)

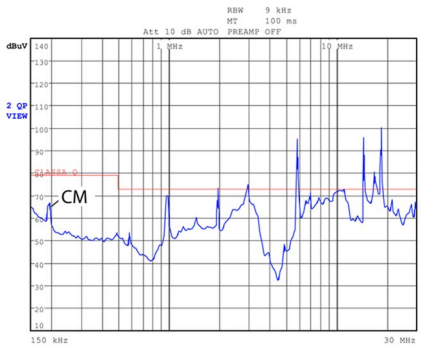

(b)

Fig. 19. (a) Arrangement of the unfavorable solid copper shield layer in the printed circuit board and (b) measured CM emissions if this shield layer is applied. The CM filter is short circuited by the shielding layer for frequencies above 5 MHz.

If the shielding layer is left open, then another effect can be observed: the copper layer covers the whole EMI filter and causes a capacitive coupling, which forms a low-impedance path bypassing the EMI filter at higher frequencies. An EMI measurement considering solely CM emissions with a copper layer beneath the whole EMI filter is given in Fig. 19(b) and verifies increased emissions. This copper layer was cut after the

CM inductors L_{CM1} for the final construction but the remaining part still caused a noise peak at 5 MHz in Fig. 15. Hence, shielding layers have to be handled with special care in order not to degrade the filter performance.

VI. Conclusion

This paper presented the design of an EMI filter for an ultracompact 10 kW three-phase/level PWM rectifier. Filter requirements have been derived using computer simulations. A specific CM filter strategy has been proposed, where the output of the rectifier shows no high-frequency CM voltage. The performance of the novel filter concept has been analyzed and the CM inductor L_{CM} turned out to be the key element for a successful implementation. An extended CM model of the rectifier system has been derived for a better understanding of CM behavior, which also demonstrated the occurrence of "MM emissions." A 10 kW laboratory prototype with a power density of 14.1 kW/dm^3 and a switching frequency of 1 MHz have been built. The performance of the designed EMI filter has been verified by measurements taken from this prototype. Modifications on several filter parts have shown that a careful component selection as well as a proper arrangement and layout is essential for achieving a satisfactory EMI filter performance.

References

[1] J. A. Rosero, J. A. Ortega, E. Aldabas, and L. Romeral, "Moving towards a more electric aircraft," *IEEE Mag. Aerosp. Electron Syst.*, vol. 22, no. 3, pp. 3–9, Mar. 2007.

[2] R. W. Erickson and D. Maksimovic, *Fundamentals of Power Electronics*, 2nd ed. New York: Springer Science+Business Media, LLC, 2001.

[3] A. Nagel and R. W. De Doncker, "Systematic design of EMI-filters for power converters," in *Proc. IEEE Industry Appl. Soc. (IAS)*, Oct., 2000, vol. 4, pp. 2523–2525.

[4] J. Biela, A. Wirthmueller, R. Waespe, M. L. Heldwein, K. Raggl, and J. W. Kolar, "Passive and active hybrid integrated EMI filters," *IEEE Trans. Power Electron.*, vol. 24, no. 5, pp. 1340–1349, May 2009.

[5] D. Zhang, D. Chen, and D. Sable, "Non-intrinsic differential mode noise caused by ground current in an off-line power supply," in *Proc. Power Electron. Spec. Conf. (PESC)*, May 17–22, 1998, vol. 2, pp. 1131–1133.

[6] S. Qu and D. Chen, "Mixed-mode EMI noise and its implications to filter design in offline switching power supplies," *IEEE Trans. Power Electron.*, vol. 17, no. 4, pp. 502–507, Jul. 2002.

[7] J. Meng and M. Weiming, "A new technique for modeling and analysis of mixed-mode conducted EMI noise," *IEEE Trans. Power Electron.*, vol. 19, no. 6, pp. 1679–1687, Nov. 2004.

[8] W. Shen, F. Wang, and D. Boroyevich, "Conducted EMI characteristic and its implications to filter design in 3-phase diode front-end converters," in *Proc. Industry Appl. Soc. (IAS)*, Oct. 3–7, 2004, vol. 3, pp. 1840–1846.

[9] W. Shen, F. Wang, D. Boroyevich, and Y. Liu, "Definition and acquisition of CM and DM EMI noise for general-purpose adjustable speed motor drives," in *Proc. Power Electron. Spec. Conf. (PESC)*, Jun.20–25, 2004, vol. 2, pp. 1028–1033.

[10] T. Nussbaumer, M. L. Heldwein, and J. W. Kolar, "Differential mode input filter design for a three-phase buck-type PWM rectifier based on modeling of the EMC test receiver," *IEEE Trans. Ind. Electron.*, vol. 53, no. 5, pp. 1649–1661, Oct. 2006.

[11] G. Laimer and J. W. Kolar, "'Zero'-ripple EMI input filter concepts for application in a 1-U 500 kHz Si/SiC three-phase PWM rectifier," in *Proc. Int. Telecommun. Energy Conf. (INTELEC)*, Oct. 19–23, 2003, pp. 750–756.

[12] H. Ye, Z. Yang, J. Dai, C. Yan, X. Xin, and J. Ying, "Common mode noise modeling and analysis of dual boost PFC circuit," in *Proc. Int. Telecommun. Energy Conf. (INTELEC)*, Sep. 19–23, 2004, pp. 575–582.

[13] S. Wang, P. Kong, and F. C. Lee, "Common mode noise reduction for boost converters using general balance technique," *IEEE Trans. Power Electron.*, vol. 22, no. 4, pp. 1410–1416, Jul. 2007.

[14] Q. Tao, J. Graham, and J. Sun, "Characterization of IGBT modules for system EMI simulation," in *Proc. 25th Appl. Power Electron. Conf. Exp.*, Feb. 21–25, 2010, pp. 2220–2225.

[15] R. Zhang, X. Wu, and T. Wang, "Analysis of common mode EMI for three-phase voltage source converters," in *Proc. 34th Power Electron. Spec. Conf.*, Jun. 15–19, 2003, vol. 4, pp. 1510–1515.

[16] Y. Zhao, Y. Li, and T. A. Lipo, "Force commutated three level boost type rectifier," *IEEE Trans. Ind. Appl.*, vol. 31, no. 1, pp. 155–161, Jan./Feb. 1995.

[17] J. W. Kolar, U. Drofenik, J. Minibock, and H. Ertl, "A new concept for minimizing high-frequency common-mode EMI of three-phase PWM rectifier systems keeping high utilization of the output voltage," in *Proc. Appl. Power Electron. Conf. (APEC)*, 2000, vol. 1, pp. 519–527.

[18] M. L. Heldwein and J. W. Kolar, "Impact of EMC filters on the power density of modern three-phase PWM converters," *IEEE Trans. Power Electron.*, vol. 24, no. 6, pp. 1577–1588, Jun. 2009.

[19] H. Joergensen, S. Guttowski, and K. Heumann, "Comparison of methods to reduce the common mode noise emission of PWM voltage-fed inverters," in *Proc. 37th Int. Power Conf.*, Nuremberg, Germany, May 26–28, 1998, pp. 273–280.

[20] F. D. Torre, S. Leva, and A. P. Morando, "A physical decomposition of three-phase variables into common and differential mode quantities," in *Proc. Int. Symp. Electromagn. Compat.*, Zurich, Switzerland, Sep. 24–28, 2007, pp. 127–130.

[21] A. Consoli, G. Oriti, A. Testa, and A. L. Julian, "Induction motor modeling for common mode and differential mode emission evaluation," in *Proc. Industry Appl. Soc. (IAS)*, Oct. 6–10, 1996, vol. 1, pp. 595–599.

[22] IEC International Special Committee on Ratio Interference—C.I.S.P.R.(2004), "Specification for Industrial, scientific and medical (ISM) radio-frequency equipment—Electromagnetic disturbance characteristics—Limits and methods of measurement—Publication 11," Geneve, Switzerland.

[23] K. Raggl, T. Nussbaumer, and J. W. Kolar, "Guideline for a simplified differential mode EMI filter design," *IEEE Trans. Ind. Electron.*, vol. 57, no. 3, pp. 1031–1040, Mar. 2010.

[24] D. G. Holmes, "A general analytical method for determining the theoretical harmonic components of carrier based PWM strategies," in *Proc. 33rd IAS Ind. Appl. Conf.*, Oct. 12–15, 1998, vol. 2, pp. 1207–1214.

[25] H. Deng, L. Helle, Y. Bo, and K. B. Larsen, "A general solution for theoretical harmonic components of carrier based PWM schemes," in *Proc. Appl. Power Electron. Conf. (APEC)*, Feb. 15–19, 2009, pp. 1698–1703.

[26] M. Odavic, M. Sumner, P. Zanchetta, and J. C. Clare, "A theoretical analysis of the harmonic content of PWM waveforms for multiple-frequency modulators," *IEEE Trans. Power Electron.*, vol. 25, no. 1, pp. 131–141, Jan. 2010.

[27] M. L. Heldwein and J. W. Kolar, "Design of minimum volume input filters for an ultra compact three-phase PWM rectifier," in *Proc. 9th Brazilian Power Electron. Conf. (COBEP)*, vol. 1, pp. 454–461, 2007.

[28] M. Schutten, "EMI causes, measurement and reduction techniques for switch-mode power converters," in *Prof. Educ. Semin. APEC*, Feb. 21–25, 2010, vol. 3, pp. 1–43, Seminar 13.

[29] M. Hartmann, A. Musing, and J. W. Kolar, "Switching transient shaping of RF power MOSFETs for a 2.5 MHz, three-phase PFC," in *Proc. Int. Conf. Power Electron. (ICPE)*, Oct. 22–26, 2007, pp. 1160–1166.

[30] M. L. Heldwein, T. Nussbaumer, F. Beck, and J. W. Kolar, "Novel three-phase CM/DM conducted emissions separator," in *Proc. Appl. Power Electron. Conf. (APEC)*, Mar. 6–10, 2005, vol. 2, pp. 797–802.

[31] Omicron electronics. (2008). Handbook of the network vector analyzer: Bode100 [Online]. Available: www.omicron-labs.com

[32] IEC International Special Committee on Ratio Interference - C.I.S.P.R.(1977), "C.I.S.P.R. Specification for Radio Interference Measuring Apparatur and Measurement Methods - Publication 16," Geneve, Switzerland.

[33] S. Wang, F. C. Lee, D. Y. Chen, and W. G. Odendaal, "Effects of parasitic parameters on EMI filter performance," *IEEE Trans. Power Electron.*, vol. 19, no. 3, pp. 869–877, May 2004.

[34] S. Wang, F. C. Lee, and J. D. van Wyk, "A study of integration of parasitic cancellation techniques for EMI filter design with discrete components," *IEEE Trans. Power Electron.*, vol. 23, no. 6, pp. 3094–3102, Nov. 2008.

[35] H. Chen, Z. Qian, Z. Zeng, and C. Wolf, "Modeling of parasitic inductive couplings in a pi-shaped common mode EMI filter," *IEEE Trans. Electromagn. Compat.*, vol. 50, no. 1, pp. 71–79, Feb. 2008.

Michael Hartmann (S'08) received the B.S. and M.Sc. degrees (Hons.) in electrical engineering from the University of Technology Vienna, Vienna, Austria, in 2005 and 2006, respectively. He is currently working toward the Ph.D. degree at the Power Electronic Systems Laboratory, Swiss Federal Institute of Technology, Zurich, Switzerland.

Currently, he is involved in the research on active three-phase rectifiers with ultrahigh switching frequencies at the Power Electronic Systems Laboratory, Swiss Federal Institute of Technology. Earlier, he was involved in the research on switched-mode power amplifiers using multicell topologies.

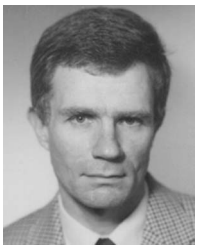

Hans Ertl (M'93) received the Dipl.-Ing. (M.Sc.) and Ph.D. degrees in industrial electronics from the University of Technology Vienna, Vienna, Austria, in 1984 and 1991, respectively.

Since 1984, he has been with the Vienna University of Technology, where he is currently an Associate Professor with the Power Electronics Section of the Institute of Electrical Drives and Machines. He has performed numerous industrial and scientific research projects in the areas of field-oriented control of ac-drive systems, switch-mode power supplies for welding and industrial plasma processes, and active rectifier systems. He is the author or coauthor of numerous scientific papers and patents. His current research interests include switch-mode power amplifiers and multicell topologies, in particular, for the generation of testing signals, for active ripple current compensators, and for several applications in the area of renewable energy systems.

Johann W. Kolar (F10) received the M.Sc. and Ph.D. degrees (*summa cum laude/promotio sub auspiciis praesidentis rei publicae*) from the University of Technology Vienna, Vienna, Austria.

Since 1984, he has been working as an Independent International Consultant in close collaboration with the University of Technology Vienna, in the fields of power electronics, industrial electronics, and high performance drives. He has proposed numerous novel PWM converter topologies, and modulation and control concepts, e.g., the Vienna rectifier and the three-phase ac–ac sparse matrix converter. He is the author or coauthor of more than 350 scientific papers in international journals and conference proceedings and has filed 75 patents. He was appointed Professor and Head of the Power Electronic Systems Laboratory at the Swiss Federal Institute of Technology (ETH), Zurich, Switzerland, on February 1, 2001. His current research interests include ac–ac and ac–dc converter topologies with low effects on the mains, e.g., for power supply of data centers, more-electric-aircraft, and distributed renewable energy systems, the realization of ultracompact and ultra-efficient converter modules employing latest power semiconductor technology (e.g., SiC), novel concepts for cooling and EMI filtering, multidomain/scale modeling/simulation and multiobjective optimization, physical model-based lifetime prediction, pulsed power, and ultrahigh speed and bearingless motors.

Dr. Kolar is a member of the Institute of Electrical Engineers of Japan (IEEJ) and of International Steering Committees and Technical Program Committees of numerous international conferences in the field (e.g., Director of the Power Quality Branch of the International Conference on Power Conversion and Intelligent Motion). From 1997 to 2000, he was an Associate Editor of the IEEE TRANSACTIONS ON INDUSTRIAL ELECTRONICS and, since 2001, he has been an Associate Editor of the IEEE TRANSACTIONS ON POWER ELECTRONICS. Since 2002, he also has been an Associate Editor of the Journal of Power Electronics of the Korean Institute of Power Electronics and a member of the Editorial Advisory Board of the IEEJ Transactions on Electrical and Electronic Engineering. He is the founding Chairman of the IEEE Power Electronics Society Austria and Switzerland Chapter and Chairman of the Education Chapter of the European Power Electronics and Drives (EPE) Association. He received the Best Transactions Paper Award of the IEEE Industrial Electronics Society in 2005, the Best Paper Award of the International Conference on Power Electronics (ICPE) in 2007, the 1st Prize Paper Award of the IEEE Industry Applications Society (IAS) Industrial Power Converters Committee (IPCC) in 2008, the IEEE Industrial Electronics Conference Best Paper Award of the Industrial Electronics Society, Power Electronics Technical Committee (IES PETC) in 2009, the 2009 IEEE Power Electronics Society Transaction Prize Paper Award and the 2010 Best Paper Award of the IEEE/ASME TRANSACTIONS ON MECHATRONICS. He also received an Erskine Fellowship from the University of Canterbury, New Zealand, in 2003. He initiated and/or is the founder/cofounder of four spin-off companies targeting ultrahigh speed drives, multidomain/level simulation, ultracompact/efficient converter systems and pulsed power/electronic energy processing. In 2006, the European Power Supplies Manufacturers Association (EPSMA) awarded the Power Electronics Systems Laboratory of ETH Zurich as the leading academic research institution in Power Electronics in Europe.